Journal of Materials Chemistry B

ROYAL SOCIETY OF CHEMISTRY

PAPER

View Article Online
View Journal | View Issue

Cite this: J. Mater. Chem. B, 2025, 13, 12224

Cyanine-scaffold fluorogenic probes for visual detection of nitroreductase in living bacteria

Jiqiang Liu, †[ace] Abdulkadir Zakari Abdulkadir,†[ab] Siye Wu,[c] Yonghui Gao,[d] Baraka Joseph Butuyuyu,[ab] Keith Man-Chung Wong,[c] Chi-Sing Lee,[e] Lintao Cai,[a] Jihong Chen[d] and Pengfei Zhang *[a]

Received 2nd April 2025,
Accepted 31st July 2025

DOI: 10.1039/d5tb00758e

rsc.li/materials-b

Bacterial infections pose significant challenges in clinical diagnostics and microbiological research due to the need for rapid, sensitive, and specific detection methods. Herein, we report the development of **Cy5-NO$_2$**, a novel nitro-containing fluorescent probe designed for real-time monitoring of bacterial nitroreductase (NTR) activity. **Cy5-NO$_2$** is synthesized through a streamlined, high-yield process without chromatography, yielding a stable compound confirmed by X-ray crystallography and spectroscopic methods. The probe exhibits negligible fluorescence in its native state but undergoes a 30-fold fluorescence enhancement at 620 nm upon NTR-mediated reduction of the nitro group to an amino group, with a detection limit of 10 ng mL^{-1}. Time-dependent density functional theory (TDDFT) calculations reveal that the fluorescence "turn-on" mechanism arises from a transition from charge-transfer quenching (in **Cy5-NO$_2$**) to local excitation (in **Cy5-NH$_2$**), as supported by a significant increase in oscillator strength. The probe demonstrates high specificity for NTR under physiological conditions and successfully detects live bacterial cells (*e.g.*, *E. coli* and *S. aureus*) *via* confocal laser scanning microscopy (CLSM). The combination of direct nitro-to-amine reduction, exceptional stability, and minimal enzymatic interference positions **Cy5-NO$_2$** as a promising tool for universal bacterial detection, advancing applications in clinical diagnostics and microbial imaging.

Introduction

Bacteria play pivotal roles in various biological processes, ranging from beneficial interactions within the human microbiome to causing severe diseases. Detecting pathogenic bacteria is crucial for diagnosing infections and guiding appropriate therapeutic interventions.[1–4] Pathogenic strains such as *Escherichia coli*, *Staphylococcus aureus*, *Klebsiella pneumoniae*, *Acinetobacter baumannii*, and *Pseudomonas aeruginosa* are responsible for significant morbidity and mortality worldwide.[5–7] Accurate identification of these pathogens is essential not only for effective treatment but also for monitoring antibiotic resistance patterns.[8,9] While traditional methods such as culture-based techniques,[10] nucleic acid amplification,[11] and mass spectrometry[12] are reliable, they are often time-consuming and resource-intensive. Therefore, there is an urgent need for innovative approaches that can quickly, sensitively, and accurately identify bacterial pathogens.

Fluorescence imaging has emerged as a powerful tool for bacterial detection due to its high sensitivity, real-time capability, and spatial resolution.[13–18] Among fluorescence-based strategies, fluorescent probes targeting nitroreductase (NTR), an enzyme highly conserved among bacteria,[19,20] offer a promising avenue for universal bacterial detection.[21,22] NTR catalyzes the reduction of nitroaromatic compounds using nicotinamide adenine dinucleotide (phosphate) (NAD(P)H) as a cofactor, making it an ideal target for developing "turn-on" fluorescence probes. These probes remain non-fluorescent until they encounter active NTR, at which point they emit a strong signal, enabling precise localization and quantification of bacterial presence. The advantage of this "turn-on" mode lies in its ability to significantly reduce background noise caused by autofluorescence or non-specific interactions, thereby enhancing detection accuracy.[23,24] However, existing

[a] Guangdong Key Laboratory of Nanomedicine, CAS-HK Joint Lab of Biomaterials, CAS Key Laboratory of Biomedical Imaging Science and System, Shenzhen Key Laboratory of Metabolic Halth, Shenzhen Metabolism and Reproductive Targeted Delivery Proof-of-Concept Center, Shenzhen Engineering Laboratory of Nanomedicine and Nanoformulations, CAS Key Lab for Health Informatics, Shenzhen Institutes of Advanced Technology, Chinese Academy of Sciences, Shenzhen, 518055, China. E-mail: pf.zhang@siat.ac.cn
[b] University of Chinese Academy of Sciences, Beijing, 100049, China
[c] Department of Chemistry, Southern University of Science and Technology, Shenzhen, 518055, China
[d] Department of Healthcare-associated Infection Control, People's Hospital of Bao'an District, Shenzhen, Shenzhen, 518101, China
[e] Department of Chemistry, Hong Kong Baptist University, Kowloon Tong, Hong Kong SAR, China
† J. Q. Liu and A.Z. Abdulkadir contributed equally to this work.

NTR-targeted fluorescent probes often suffer from limitations such as complex synthesis routes, short emission wavelengths, poor stability and insufficient sensitivity or selectivity.[25–27] Addressing these issues requires the development of new probes that are simpler to synthesize, exhibit longer emission wavelengths, are stable in biological media and demonstrate enhanced performance.

In this study, we introduce **Cy5-NO$_2$**, a novel nitro-containing fluorescent probe designed for the real-time monitoring of bacterial NTR activity. Synthesized through a straightforward and efficient process, **Cy5-NO$_2$** exhibits remarkable stability and specificity toward NTR. Upon reduction by NTR, the probe displays a 30-fold increase in fluorescence intensity at 620 nm, with a detection limit of 10 ng mL^{-1}. Unlike previously reported self-immolative cleavage-type cyanine-based probes such as heptamethine systems (Smith *et al.*), which require multi-step modifications to achieve nitroreductase responsiveness, leading to increased production costs and poor stability due to inherent polyene linkers of the heptamethine structure and hydrolyzable functional groups,[28] or "turn-off" probes like **Cy7-NO$_2$** (Sui *et al.*), which necessitate signal inversion for clinical interpretation,[29] **Cy5-NO$_2$** operates *via* direct nitro-to-amine reduction. This streamlined mechanism eliminates auxiliary functional groups, thereby avoiding interference from hydrolytic enzymes (*e.g.*, esterases/proteases) inherent to prior systems. Emitting at 620 nm, **Cy5-NO$_2$** achieves a balance between reduced autofluorescence and compatibility with standard confocal microscopy setups, enabling robust real-time imaging of live bacteria, as demonstrated by its successful application in detecting *E. coli* and *S. aureus via* confocal laser scanning microscopy. Furthermore, its minimalist design enhances stability, while column-free synthesis and cost-efficient production underscore scalability for industrial translation. These findings highlight the potential of **Cy5-NO$_2$** as a valuable tool for sensitive and specific bacterial detection and imaging, advancing microbiological research and clinical diagnostics. By overcoming the limitations of current probes, **Cy5-NO$_2$** represents a significant advancement in bacterial detection, offering enhanced sensitivity and specificity that pave the way for more effective diagnostic tools and therapeutic strategies against bacterial infections.

Results and discussion

Design and synthesis of probe Cy5-NO$_2$

Nitroaromatic compounds can serve as biomarkers for the detection of bacterial nitroreductases (NTRs), as they are enzymatically reduced to nitrile, hydroxylamine, and amino derivatives by NADH/NADPH cofactors.[30] The synthetic pathway for **Cy5-NO$_2$** is outlined in Fig. 1A. The synthesis began with **Cy5-Cl**, a near-infrared (NIR) luminescent reporter, which was reacted with acetylacetone in the presence of Et$_3$N as a catalyst to afford **Cy5-acac**. Subsequently, **Cy5-acac** underwent a heterocyclization reaction with *p*-nitroaniline, the NTR-responsive moiety, yielding the target probe, **Cy5-NO$_2$**. Notably, this final step is highly efficient, characterized by the precipitation of a blue-violet solid, which can be purified *via* simple filtration without requiring column chromatography, resulting in a reaction yield of 92%. This streamlined process ensures high reproducibility and cost-effectiveness, addressing a critical bottleneck in cyanine dye manufacturing. Blue crystals suitable for structural analysis were obtained by a diffusion system of diethyl ether and acetonitrile solution. The structure of **Cy5-NO$_2$** was fully characterized using ^{1}H NMR, ^{13}C NMR, and high-resolution mass spectrometry (HR-MS) (see the SI), providing conclusive evidence for its identity. The molecular structure of **Cy5-NO$_2$** has been detected by X-ray crystallography (XRD). The perspective drawing of **Cy5-NO$_2$** is presented in Fig. S1. The supplementary crystallographic data for **Cy5-NO$_2$** are summarized in Table S1, and the selected bond lengths (in Å) and bond angles (in degrees) of **Cy5-NO$_2$** are listed in Table S2. The benzoindole unit and the middle heterocyclic core in the **Cy5-NO$_2$** structure are nearly planar (Fig. S1). A distortion angle of 76.5° is observed between the central heterocyclic ring (C14–C15–N2–C22–C23–C24) and the *p*-nitrobenzene ring (C16–C17–C18–C19–C20–C21). This angular displacement alleviates the steric hindrance between these two rings, contributing to enhanced molecular stability. Additionally, the absence of hydrolysable moieties ensures resistance to enzymatic degradation, a critical feature for *in vivo* applications.

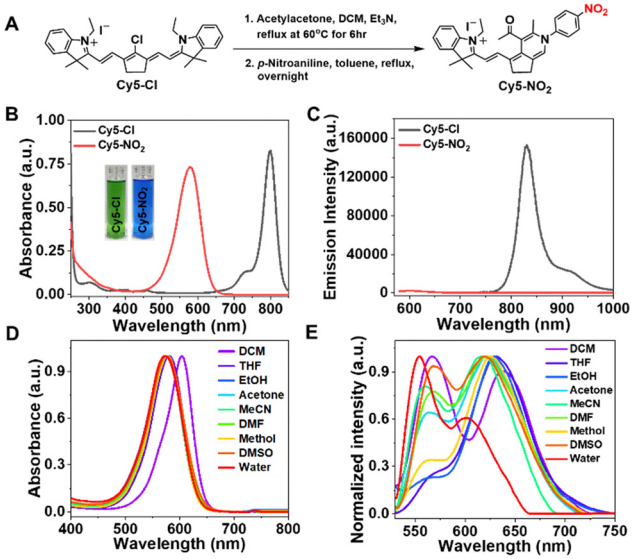

Fig. 1 (A) Synthetic route of **Cy5-NO$_2$** (probe). (B) Absorption and (C) emission spectra of **Cy5-Cl** and **Cy5-NO$_2$** in PBS buffer (10 mM, pH 7.4, 10% DMSO). Normalized absorption (D) and emission (E) spectra acquired for **Cy5-NO$_2$** in different solvents. Optical spectra were recorded at 20 μM. For emission spectra that were excited at 500 nm.

Photophysical properties of Cy5-NO$_2$

The absorption and fluorescence spectra of the NTR probes were assessed in a PBS buffer (10 mM, pH 7.4) with 10% v/v DMSO at 37 °C. As shown in Fig. 1B and C, probe **Cy5-NO$_2$** exhibited an intense absorption peak at 578 nm corresponding to the π–π* electronic transition, representing a significant blue

shift of 220 nm relative to its precursor **Cy5-Cl**. Notably, this structural modification induced dramatic fluorescence quenching, as evidenced by the markedly diminished emission intensity compared to the unmodified precursor under identical experimental conditions. Furthermore, **Cy5-NO$_2$** demonstrated pronounced sensitivity to solvent polarity, as reflected by substantial spectral shifts observed during transitions from low-polarity to high-polarity solvents (Fig. 1D, E, and Fig. S2). In weakly polar solvents such as dichloromethane (DCM), the probe displayed a pronounced bathochromic shift in its absorption spectrum ($\lambda_{abs} \approx 604$ nm) compared to polar solvents like water and dimethyl sulfoxide ($\lambda_{abs} \approx 578$ nm). The hypsochromic behavior observed across absorption, emission, and excitation profiles can be rationalized through solvation-induced stabilization mechanisms: polar solvents preferentially stabilize the polar ground-state (HOMO level) relative to the less polar first-excited state of the probe.[17,31,32] This differential stabilization increases the HOMO–LUMO energy gap, thereby inducing the observed hypsochromic shifts in the electronic spectra. These solvent-dependent spectral variations underscore the probe's structural responsiveness to environmental polarity changes through solvatochromic interactions. For potential applications in biological systems, the photostability of **Cy5-NO$_2$** was studied in phosphate-buffered saline (PBS) solution under continuous white light irradiation for 40 minutes. No significant degradation of **Cy5-NO$_2$** was observed at its characteristic absorption wavelength (578 nm) (Fig. S3). This result underscores the remarkable photostability of **Cy5-NO$_2$** in PBS media. This contrasts sharply with conventional cyanine dyes, which typically degrade rapidly due to photoisomerization[33,34] or aggregation.[35,36] The enhanced stability arises from its rigid planar structure (as confirmed by X-ray crystallography) and the reduced number of inherent polyene linkers in the heptamethine structure.[37]

NTR response of Cy5-NO$_2$ in aqueous solution

The NTR response properties of **Cy5-NO$_2$** were assessed in a PBS buffer solution (10 mM, pH 7.4, with 10% DMSO[38–40]), both in the presence and absence of NADH with a 60-minute incubation period. As shown in Fig. 2B, when either NADH (500 μM) or NTR (20 μg mL^{-1}) was individually added to the probe, no significant change was observed in the absorption peak of the

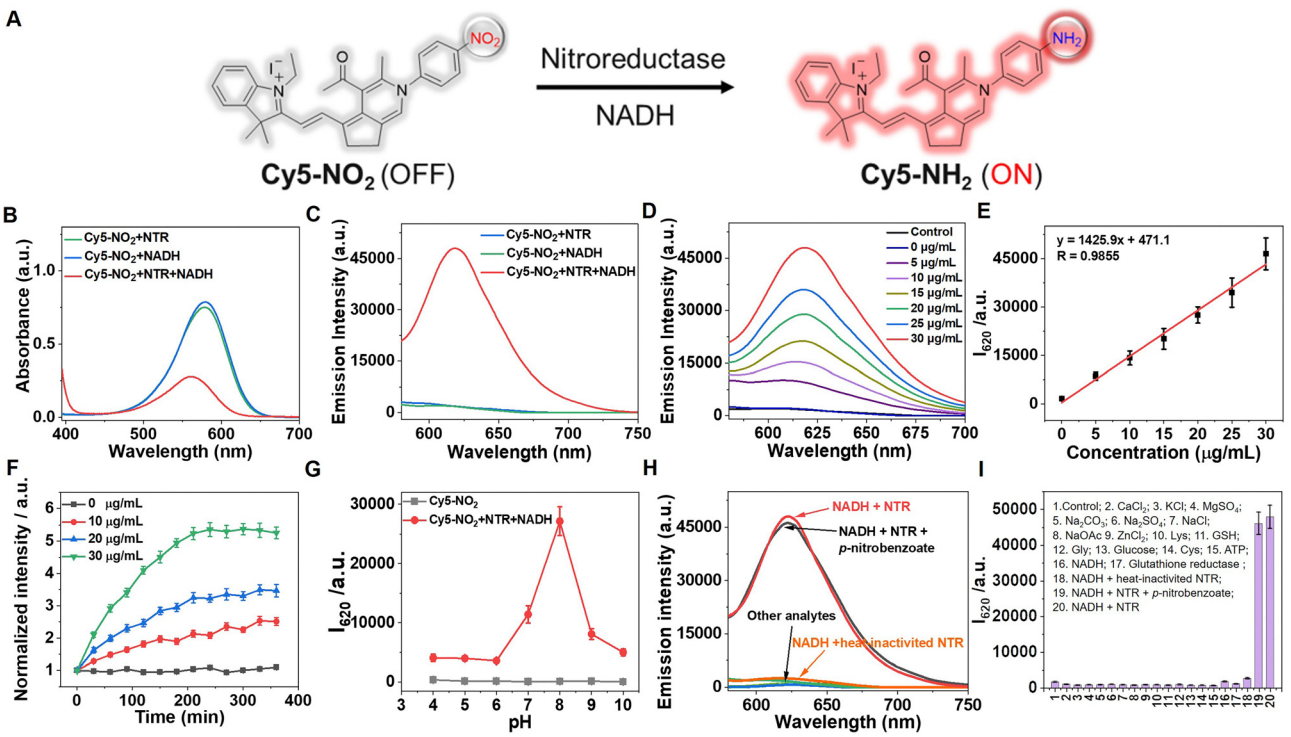

Fig. 2 (A) Proposed mechanism of **Cy5-NO$_2$**'s response to NTR activity. (B) Absorption and (C) emission spectra of **Cy5-NO$_2$** (20 μM) in PBS buffer (10 mM, pH 7.4, with 10% DMSO), measured with or without NTR (20 μg mL^{-1}) and/or NADH (500 μM). (D) Sensitivity of the **Cy5-NO$_2$** probe (20 μM) to varying concentrations of NTR (0–30 μg mL^{-1}) in PBS buffer. (E) Linear correlation between fluorescence intensity at 620 nm (I_{620nm}) and NTR concentrations in the presence of NADH after 60 min incubation at 37 °C. (F) Normalized time-dependent fluorescence changes of **Cy5-NO$_2$** (20 μM) in the presence of varying NTR concentrations (0, 10, 20, and 30 μg mL^{-1}). (G) Emission intensity of the **Cy5-NO$_2$** probe (20 μM) at 620 nm across different pH values in the presence of NTR (20 μg mL^{-1}) and NADH (500 μM) incubated in Britton–Robinson buffer solution at 37 °C for 60 min. (H) and (I) Emission intensity (I_{620nm}) of **Cy5-NO$_2$** (20 μM) with different analytes (100 μM each) after 60 min incubation at 37 °C in the presence of NTR (20 μg mL^{-1}). Analytes include: 1. Blank, 2. $CaCl_2$, 3. KCl, 4. $MgSO_4$, 5. Na_2CO_3, 6. Na_2SO_4, 7. NaCl, 8. NaOAc, 9. $ZnCl_2$, 10. lysine (Lys), 11. glutathione (GSH), 12. glycine (Gly), 13. glucose, 14. cysteine (Cys), 15. ATP, 16. NADH, 17. glutathione reductase, 18. NADH +heat-inactivated NTR, 19. NADH + NTR + excess *p*-nitrobenzoate (a substrate analogue as competitor) and 20. NADH + NTR, λ_{ex} = 500 nm. Data represent mean values from three independent experiments. Error bars denote standard deviation (±SD).

Table 1 Fluorescence quantum yields of **Cy5-NO$_2$** under different solvent conditions in the absence and presence of NTR and NADH

Φ_{Fl}	PBS (pH 7.4)	10% DMSO[a]	50% DMSO[a]	Pure DMSO	Pure EtOH	Pure THF	Pure DCM
Without NTR[b]	0.001	0.001	0.003	0.01	0.015	0.016	0.004
Φ_{Fl}	**PBS (pH 7.4)**	**10% DMSO[a]**	**50% DMSO[a]**	**80% DMSO[d]**	**80% EtOH[d]**	**80% THF[d]**	**80% DCM[d]**
With NTR[bc]	0.022	0.093	0.068	0.03	0.028	0.026	0.009

[a] All solvent volumes were adjusted to the same final volume using PBS. [b] The solutions containing **Cy5-NO$_2$** (20 μM) were incubated at 37 °C for 60 min. [c] This condition was tested in the presence of NTR (20 μM) and NADH (500 μM). [d] The solution was prepared by 0.8 mL NTR (100 μg mL^{-1} in water) with 3.2 mL pure organic solvent.

reaction system, which remained centered around 578 nm. However, its absorption was blue-shifted to 562 nm, which was triggered by the presence of both NTR and NADH. Additionally, under 500 nm excitation, no apparent change in fluorescence intensity was observed upon individual addition of NADH or NTR. Consistent with the absorption spectra, a significant enhancement in fluorescence emission (approximately 30-fold) centered at 620 nm was observed when both NTR and NADH were added (Fig. 2C). This suggests that the observed fluorescence enhancement is attributable to the NTR-catalyzed reduction of the nitro group in the presence of NADH, yielding the reduced product **Cy5-NH$_2$** (Fig. 2A), a transformation corroborated by HR-ESI-MS analysis that detected the corresponding $[M + H]^+$ ion at *m/z* 464.2698 (Fig. S4). These results further confirm that the "turn-on" fluorescence of the probe is attributed to the catalytic reduction of the nitro group by NTRs.

To evaluate the sensitivity of the **Cy5-NO$_2$** probe toward NTR, fluorescence spectra were recorded at NTR concentrations from 0 to 30 μg mL^{-1} (in 5 μg mL^{-1} increments). As the NTR concentration increased, the fluorescence intensity at 620 nm (I_{620nm}) gradually enhanced, peaking at 30 μg mL^{-1} (Fig. 2D). The plot of I_{620nm} against NTR concentration showed a strong linear relationship within 0–30 μg mL^{-1} (Fig. 2E). Based on the formulae for the limit of detection (LOD = $3\sigma/k$) and limit of quantification (LOQ = $10\sigma/k$), where σ represents the standard deviation of the blank signal and k is the slope of the calibration curve, the LOD and LOQ were determined to be 10 ng mL^{-1} and 33.3 ng mL^{-1}, respectively. These results demonstrate the probe's high sensitivity, enabling precise and quantitative detection of NTR at low concentrations.

Fluorescence quantum yield measurements

Absolute fluorescence quantum yield measurements of **Cy5-NO$_2$** were conducted both in the absence and presence of NTR and NADH across seven solvent systems to evaluate the probe's behavior under varying conditions. In the absence of NTR and NADH, **Cy5-NO$_2$** exhibited strong fluorescence quenching ($\Phi_{Fl} < 0.003$) in aqueous or low-DMSO environments (<50%), primarily attributed to efficient intramolecular charge transfer (ICT), which dominates non-radiative decay pathways. Similarly, in low-polarity solvents such as DCM, the quantum yield remained low due to stabilization of the charge-transfer state, consistent with the observed red shift in the absorption spectrum compared to other solvents. In contrast, more polar organic solvents yielded Φ_{Fl} values between 0.01 and 0.016, indicating partial suppression of the ICT process.

In the presence of NTR and NADH, a significant increase in quantum yield was observed, confirming the enzymatic reduction of the nitro group and the subsequent "turn-on" fluorescence response of **Cy5-NH$_2$**. Among all tested conditions, the highest quantum yield (Φ_{Fl} = 0.093) was achieved in PBS containing 10% DMSO (Table 1). Increasing the DMSO concentration to 50% resulted in an ~27% decrease relative to the peak value, while at 80% DMSO, the quantum yield dropped by ~70%. A similar sharp decline was observed in other high-concentration organic solvent systems (*e.g.*, 80% ethanol or 80% THF in PBS). This reduction is likely linked to structural disruption or denaturation of the enzyme, leading to markedly reduced catalytic activity. The relatively low quantum yield in pure PBS (Φ_{Fl} = 0.022) may stem from poor probe solubility, which was significantly improved by the addition of 10% DMSO. These findings not only provide deeper insight into the photophysical behavior of **Cy5-NO$_2$** but also support its reliability and performance in complex biological environments.

Dynamic studies of Cy5-NO$_2$

To evaluate the kinetic properties of **Cy5-NO$_2$**, changes in fluorescence intensity at 620 nm (I_{620} nm) were monitored over time (0–360 min) at various NTR concentrations (0–30 μg mL^{-1}) in the presence of NADH (Fig. 2F). Upon adding NTR, the fluorescence intensity at 620 nm increased gradually and stabilized by approximately 200 min, demonstrating the probe's reliability for NTR detection.

Effect of pH on Cy5-NO$_2$

The fluorescence response of a probe can be significantly influenced by pH levels. Therefore, an investigation was conducted to assess how pH variations impact the emission intensity at 620 nm of **Cy5-NO$_2$** (Fig. 2G). In the presence of NTR and NADH, **Cy5-NO$_2$** demonstrated significant fluorescence emission over a pH ranging from 6 to 10, with its efficiency peaking around pH 8.0. Considering the practical application of the probe in biological systems, a pH of 7.4 was chosen for all subsequent experiments.

Selectivity

The selectivity of **Cy5-NO$_2$** for NTR was evaluated by comparing its response to various substances, including inorganic salts, amino acids, reductive agents, sugars, thiol-containing compounds, unrelated enzymes, substrate analogues for competing

and heat-inactivated NTR. As demonstrated in Fig. 2H and I, **Cy5-NO$_2$** exhibited a pronounced fluorescence enhancement at 620 nm exclusively in the combined presence of NTR and NADH. Notably, co-incubation of the probe with NTR, NADH, and *p*-nitrobenzoate (a substrate analogue) at equimolar concentrations showed no significant difference in fluorescence intensity compared to the system without the analogue, confirming that the enzymatic catalysis of the probe remains unaffected by the presence of structurally related molecules. Furthermore, thermal inactivation of NTR through heating at 80 °C for 30 minutes completely abolished the fluorescence enhancement, confirming the enzymatic activity dependence of the response. Control experiments revealed negligible fluorescence changes in the presence of individual components (NTR or NADH) or other tested substances, underscoring the system's high selectivity. These findings collectively establish **Cy5-NO$_2$** as a highly specific fluorescent probe for NTR detection, with robust resistance to both competitive inhibition and non-specific interactions, thereby ensuring reliable and accurate enzymatic sensing.

Calculation study

To investigate the mechanism underlying the fluorescence changes of **Cy5-NO$_2$** and its product **Cy5-NH$_2$** upon reaction with NTR, we performed time-dependent density functional theory (TDDFT) calculations. As depicted in Fig. 3, in the excited state of **Cy5-NO$_2$**, the highest occupied molecular orbital (HOMO) is predominantly localized on the benzoindole and the middle heterocyclic moiety, whereas the lowest unoccupied molecular orbital (LUMO) is only situated within the nitrobenzene unit. This spatial separation between the HOMO and LUMO results in significant charge transfer, which effectively quenches fluorescence. In contrast, after reduction by NTR, the transformation of **Cy5-NO$_2$** into **Cy5-NH$_2$** leads to a redistribution of the frontier orbitals. Both the HOMO and LUMO are confined to the benzoindole and the middle heterocyclic region, corresponding to a local excitation (LE) state. This transition promotes substantial fluorescence emission. Consistent with this observation, the calculated oscillator strength (*f*) for **Cy5-NH$_2$** is 0.8750, markedly higher than that of **Cy5-NO$_2$** (0.0014), further corroborating the observed enhancement in fluorescence.

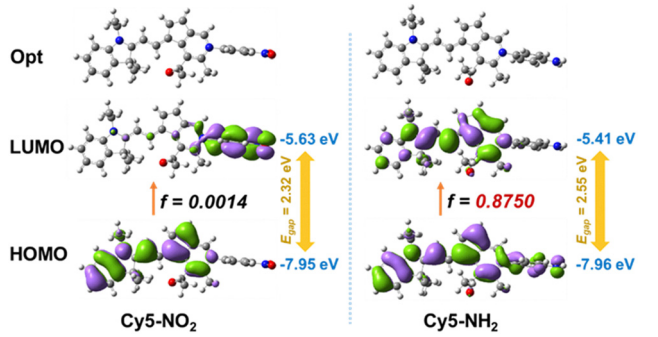

Fig. 3 The HOMO/LUMO frontier molecular orbitals and oscillator strength (f) calculated by TDDFT of **Cy-NO$_2$** (left) and **Cy-NH$_2$** (right) under the singlet excited states, respectively.

Inhibitory test of NTR activity

Dicoumarol(Dic), a competitive inhibitor of NADH, was employed to suppress NTR activity allowing the evaluation of the detection efficacy of NTR probes. Upon addition of 300 μM dicoumarol, a notable decrease in the fluorescence signal of the probe was observed (Fig. S5). This result verifies that the fluorogenic response of the NTR probes is exclusively dependent on the presence of active NTR enzymes.

Bacterial detection by the NTR probe

NTRs are universally present in bacteria. Due to the probe's strong responsiveness to NTR, making it suitable for fluorescence imaging as a "turn-on" probe, we propose its use for detecting bacterial nitroreductases produced during bacterial growth. *E. coli* and *S. aureus* were chosen as model pathogenic bacteria for the experiment. To determine the optimal concentration for bacterial detection, we evaluated the fluorescence behavior of the probe across a range of concentrations (Fig. 4A and B). The results demonstrated a concentration-dependent increase in fluorescence intensity, with *E. coli* exhibiting the most pronounced response. Considering both the need for sufficient signal strength and the desire to minimize probe usage, 20 μM was selected as the optimal concentration for subsequent experiments, as it provided robust fluorescence while avoiding excessive reagent consumption. Furthermore,

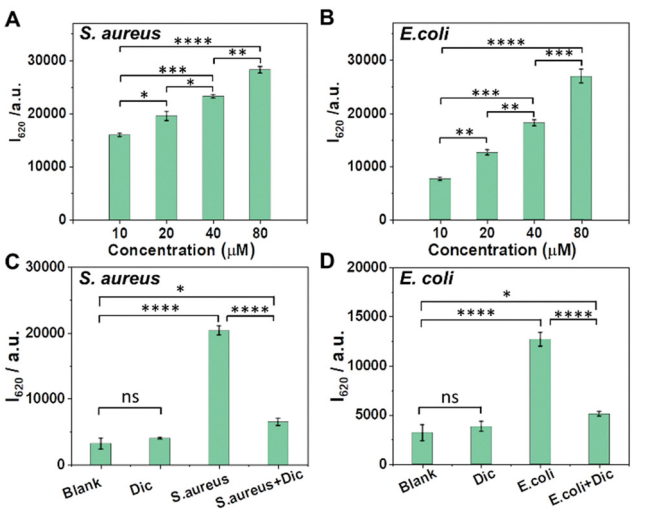

Fig. 4 Fluorescence detection of live bacteria using **Cy5-NO$_2$**. Fluorescence measurements were carried out after incubating (A) *S. aureus* and (B) *E. coli* with varying concentrations of **Cy5-NO$_2$**, or (C) *S. aureus* and (D) *E. coli* with 20 μM **Cy5-NO$_2$** in the presence or absence of 0.1 mM Dic, for 60 min at 37 °C. Fluorescence was measured at λ_{ex} = 500 nm and λ_{em} = 620 nm. This assay demonstrates the response of live bacterial cells to **Cy5-NO$_2$** under different experimental conditions. Blank group means **Cy5-NO$_2$** in PBS without bacteria. Error bars represent standard deviation (n = 3 independent replicates). Statistical significance was calculated *via* Student's *t*-test, ****p < 0.0001, *p < 0.05, p > 0.05 not considered statistically significant (ns).

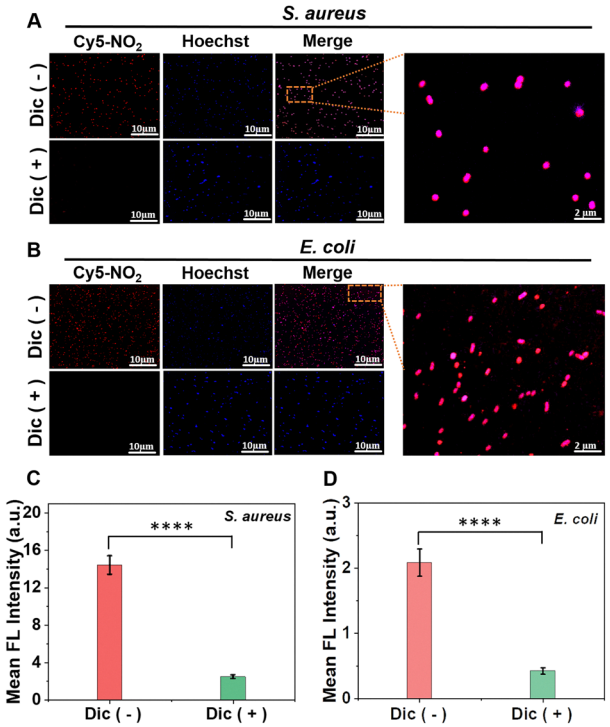

Fig. 5 Confocal laser scanning microscopy images of **Cy5-NO$_2$** (20 μM) co-incubated with (A) *S. aureus* and (B) *E. coli*, both in the absence and presence of 0.1 mM Dic for 60 min at 37 °C. Panels (C) and (D) display the corresponding mean fluorescence intensities of the red channel. Fluorescence intensity measurements of **Cy5-NO$_2$** in bacterial cells. Imaging experiments were conducted using excitation/emission wavelength pairs of 405 nm/410–480 nm for Hoechst and 552 nm/600–650 nm for **Cy5-NO$_2$**. The laser power was set at 10% for Hoechst and 15% for **Cy5-NO$_2$** to minimize photobleaching. Fluorescence intensities were quantified from the bacteria in the image by ImageJ software. Error bars represent standard deviation (n = 3 independent replicates). Statistical significance was calculated *via* Student's t-test, ****$p < 0.0001$. Scale bar: 10 μm.

to confirm the specificity of the probe toward nitroreductase (NTR) activity, we performed additional experiments using Dic. The emission intensity of the bacteria was measured after incubation with the probe, both in the presence and absence of Dic (Fig. 4C and D). The results revealed a significant increase in the fluorescence intensity of **Cy5-NO$_2$** following incubation with different bacterial strains, surpassing the control group. However, upon adding Dic to the bacterial solution, the fluorescence intensity decreased to the level of the control group, indicating that the fluorescence was directly linked to the enzymatic activity of NTRs in the bacteria. Taken together, these findings validate the probe's efficacy and specificity for nitroreductase detection in bacteria, and we propose that 20 μM can be the optimal concentration of **Cy5-NO$_2$** for bacterial imaging.

Detection limits of the NTR probe

To determine the minimum detectable colony-forming unit (CFU) of **Cy5-NO$_2$**, its response was evaluated toward pathogenic *E. coli* (Gram-negative), *S. aureus* (Gram-positive), and methicillin-resistant *S. aureus* (MRSA). Bacterial cultures were incubated with **Cy5-NO$_2$** (20 μM for 1 h), and fluorescence intensity at 620 nm was quantified. A dose-dependent increase in fluorescence was observed across all three bacterial strains as CFU concentrations increased (Fig. S6). Notably, **Cy5-NO$_2$** exhibited a significant fluorescence response at 3×10^6 CFU mL^{-1} for *E. coli* and *S. aureus*, whereas MRSA required a higher detection threshold of 5×10^6 CFU mL^{-1}. This sensitivity profile highlights the potential of **Cy5-NO$_2$** as a diagnostic tool for bacterial infections, particularly in clinical settings where rapid identification of both Gram-negative and Gram-positive pathogens is crucial. The ability to detect MRSA at clinically relevant concentrations further underscores its applicability in monitoring antibiotic-resistant infections, which are associated with high morbidity and mortality in hospital settings. This discrepancy may be attributed to MRSA-specific features, such as enhanced cell wall rigidity or altered enzymatic activity, which could hinder the probe's interaction with the bacterial target.[41]

Bacterial imaging and visual detection by the NTR probe

To visualize the detection of live bacterial cells with the probe, a confocal laser scanning microscope (CLSM) was utilized. Hoechst dye was utilized to stain live bacterial DNA, emitting blue fluorescence, while the probe generated red fluorescence through its interaction with bacterial NTRs. As illustrated in Fig. 5A and B, robust red fluorescence was observed for both *E. coli* and *S. aureus* bacterial strains. Notably, in the groups pre-incubated with Dic, the red fluorescence intensity was significantly quenched, confirming that the red fluorescence was indeed due to the catalytic reduction of **Cy5-NO$_2$** by bacterial NTRs (Fig. 5C and D). These findings highlight that **Cy5-NO$_2$** holds great potential as a "turn-on" probe for detecting and imaging live bacterial cells with a strong fluorescence response.

Conclusions

In summary, we have developed **Cy5-NO$_2$**, a highly sensitive and selective fluorescent probe for real-time monitoring of bacterial nitroreductase (NTR) activity. This probe operates *via* a streamlined mechanism of direct nitro-to-amine reduction, eliminating auxiliary functional groups that are prone to hydrolytic enzyme interference, such as esterases or proteases, which are common limitations in prior systems. The design of **Cy5-NO$_2$** ensures exceptional stability, as evidenced by its resistance to degradation under continuous irradiation and its rigid planar structure confirmed by X-ray crystallography. Upon NTR-mediated reduction, the probe exhibits a dramatic 30-fold fluorescence enhancement at 620 nm, with a detection limit of 10 ng mL^{-1}, demonstrating improved performance in sensitivity and stability compared to most previously reported NTR-targeted probes. Time-dependent density functional theory (TDDFT) calculations reveal that this "turn-on" mechanism arises from a transition from charge-transfer quenching in

the nitro form (**Cy5-NO$_2$**) to local excitation in the reduced amine form (**Cy5-NH$_2$**), supported by a calculated oscillator strength increasing from 0.0014 to 0.8750. High-resolution mass spectrometry (HR-MS) analysis confirms the formation of **Cy5-NH$_2$** post-reduction, validating the theoretical predictions. The probe's high specificity for NTR under physiological conditions and its compatibility with standard confocal microscopy enable robust detection and imaging of live bacterial cells, such as *E. coli* and *S. aureus*, as demonstrated by confocal laser scanning microscopy (CLSM). Furthermore, its column-free synthesis (92% yield) and minimal enzymatic interference position it as a scalable platform for industrial translation. These features collectively highlight **Cy5-NO$_2$** as a transformative tool for sensitive and specific bacterial detection, addressing critical gaps in current technologies and advancing applications in clinical diagnostics, microbial imaging, and targeted antimicrobial strategies.

Experimental

Materials and instruments

Unless otherwise stated, all solvents and reagents were commercially available and used without further purification. *Escherichia coli* nitroreductase (NTR) was obtained from Shanghai yuanye Bio-Technology Co., Ltd. The NTR was dissolved in ultrapure water (Milli-Q IQ 700), and the resulting enzyme solution was immediately stored at −22 °C to preserve enzyme activity. Additionally, NTR was dissolved in ultrapure water to prepare a stock solution of 100 μg mL^{-1} for subsequent use. β-Nicotinamide adenine dinucleotide (NAD) hydrogen salt (NADH) was also obtained from Shanghai yuanye Bio-Technology Co., Ltd. High-resolution mass spectra were acquired using a Q-Exactive Hybrid quadrupole-Orbitrap mass spectrometer. The ^{1}H NMR and ^{13}C NMR spectra were recorded on a Bruker AVANCE III 400 MHz and a Bruker AVANCE 101 Digital NMR Spectrometer, respectively, using CD_3CN-d_3 as the solvent and tetramethylsilane (TMS) as the internal reference. UV-vis absorption spectra were recorded on a SuperMax 2800MF UV-vis spectrophotometer, and fluorescence spectra were measured on a FL970 Fluorescence spectrophotometer with a 1 cm standard quartz cell. Confocal microscopy images of *E. coli* and *S. aureus* were acquired using a Leica LAS X confocal microscope. All bacterial strains used in this study were purchased from ATCC.

Spectral measurements

All spectral measurements were performed under standardized conditions. A stock solution of **Cy5-NO$_2$** (10.0 mM) was prepared with DMSO and NADH (10.0 mM) was dissolved in ultrapure water. For the assay, NTR was dissolved in ultrapure water to the desired concentration. A working solution containing **Cy5-NO$_2$** (20 μM) and NADH (500 μM) was prepared in 10 mM PBS buffer (pH 7.4) with 10% DMSO. The varying concentrations of NTR (0–30 μg mL^{-1}) were added to the mixture, which was then incubated at 37 °C for 60 minutes. The spectra were recorded at an excitation wavelength of 500 nm after thorough mixing and incubation. All photophysical experiments were conducted in triplicate using independent sample preparations. Data are expressed as mean ± standard deviation (SD).

Fluorescence quantum yield measurements

The absolute fluorescence quantum yield (Φ_{Fl}) of **Cy5-NO$_2$** was measured using a Hamamatsu C11347 Absolute Photoluminescence Quantum Yield Measurement System under two experimental conditions: (1) in the absence of NTR and NADH, and (2) in the presence of NTR (20 μM) and NADH (500 μM). For the first condition, seven solvent systems containing 20 μM **Cy5-NO$_2$** were prepared, including PBS (pH 7.4), PBS with 10% or 50% DMSO, pure DMSO, pure ethanol, pure tetrahydrofuran (THF), and pure dichloromethane (DCM). For the second condition, the stock NTR solution (100 μg mL^{-1} in water) was pre-mixed with organic solvents to achieve final concentrations of 20 μM NTR, and seven solvent systems containing 20 μM **Cy5-NO$_2$** were prepared in a total volume of 4 mL as follows: PBS (3.2 mL PBS + 0.8 mL NTR + 1.42 mg NADH), 10% DMSO (2.8 mL PBS + 0.4 mL DMSO + 0.8 mL NTR + 1.42 mg NADH), 50% DMSO (1.2 mL PBS + 2.0 mL DMSO + 0.8 mL NTR + 1.42 mg NADH), 80% DMSO (3.2 mL DMSO + 0.8 mL NTR + 1.42 mg NADH), 80% ethanol (3.2 mL ethanol + 0.8 mL NTR + 1.42 mg NADH), 80% THF (3.2 mL THF + 0.8 mL NTR + 1.42 mg NADH), and 80% DCM (3.2 mL DCM + 0.8 mL NTR + 1.42 mg NADH). All samples were incubated at 37 °C for 60 minutes to ensure complete enzymatic reduction of **Cy5-NO$_2$** to **Cy5-NH$_2$** prior to quantum yield measurements.

Selectivity, pH influence and dynamic study of the probe

To evaluate the specificity of the probe for NTR, it was incubated with various species (100 μM each: NaCl, KCl, $ZnCl_2$, Na_2CO_3, Na_2SO_4, NaOAc, $CaCl_2$, $MgSO_4$, cysteine, lysine, glycine, glutathione, glucose, ATP (adenosine triphosphate), NADH, glutathione reductase, NADH + heat-inactivated NTR (heat at 80 °C for 30 min), NADH + NTR + excess *p*-nitrobenzoate (a substrate analogue as competitor) and (NADH + NTR)) in PBS/DMSO at 37 °C for 60 minutes. The influence of pH on probe responsiveness to NTR was studied by measuring photoluminescence at varying pH levels (4–10) using the probe (20 μM) with NTR (20 μg mL^{-1}) and NADH (500 μM) incubated in Britton–Robinson buffer solution at 37 °C for 60 min. Kinetic properties were examined by monitoring fluorescence intensity changes over time for **Cy5-NO$_2$** (20 μM) with varying NTR concentrations (0–30 μg mL^{-1}). All spectra were recorded at 500 nm excitation after mixing and incubation. The selectivity experiment was conducted in triplicate using independent sample preparations. Data are expressed as mean ± standard deviation (SD).

Sensing mechanism of Cy5-NO$_2$ with NTR

To further verify this reduction process, we performed high-resolution mass spectrometry on the reaction mixture after treatment with NTR/NADH. Specifically, **Cy5-NO$_2$** (20 μM),

NADH (500 μM) and NTR (20 μg mL^{-1}) were incubated in PBS buffer (10 mM, pH 7.4) at 37 °C for 60 min. After completion of the reaction, the mixture was extracted with dichloromethane (3 × 20 mL), dried over anhydrous sodium sulfate, and concentrated under reduced pressure. The resulting residue was analyzed by HR-ESI-MS, which clearly showed a molecular ion ($[M + H]^+$) peak at *m/z* 464.2698.

Bacteria detection and imaging

Bacterial suspensions of *Escherichia coli* (*E. coli*) and *Staphylococcus aureus* (*S. aureus*) were treated with **Cy5-NO$_2$** (20 μM) for 60 min at 37 °C, both with and without Dic (0.1 mM), an NTR inhibitor. After incubation, fluorescence was measured to assess probe activation. Bacterial cells were cultured, treated with probes (20 μM) and Dic (0.1 μM), and incubated for 60 min at 37 °C. Cells were harvested by centrifugation, washed twice with Tris–HCl buffer (50 mM, pH 7.4), and resuspended in PBS at one-tenth the original volume. The bacteria were then stained with Hoechst (3 μM) for 5 min, washed twice, and resuspended in PBS. A suspension of stained cells was placed on a confocal dish and immobilized with an agar block for imaging. Confocal microscopy images were obtained using a LAS X confocal microscope equipped with a 63× oil immersion objective lens. Two imaging channels were employed: channel 1 (Hoechst 33342) was excited at 405 nm with emission detected between 410 and 480 nm (blue channel) and channel 2 (**Cy5-NO$_2$**) utilized an excitation wavelength of 552 nm and emission detection at 600–650 nm (red channel). Image acquisition was performed in 3D *z*-stack mode (5 slices, 0.5 μm step size) with a pixel resolution of 1024 × 1024. To minimize photobleaching, laser power was set to 10% for Hoechst 33342 and 15% for **Cy5-NO$_2$**. Hoechst 33342 was used to visualize bacterial DNA, while **Cy5-NO$_2$** was employed to monitor the fluorescent response of the probe. This protocol enabled clear and reliable analysis of bacterial samples. Post-acquisition image processing was conducted using LAS X v3.7 software.

Computational calculations

All the theoretical calculations were performed using the density functional theory (DFT) and time-dependent density functional theory (TD-DFT) based on B3LYP/6-31G(d,p) basis set, which were performed on Gaussian 09 software package.

Statistical analysis

All experiments were performed three times and the data were presented as mean ± standard deviation. Statistical analysis was performed according to the Student's *t*-test and one-way ANOVA analysis. Differences were considered statistically significant at the following *p* values: $*p < 0.05$, and $****p < 0.0001$, $p > 0.05$ not considered statistically significant (ns).

Synthesis of Cy5-acac

Synthesis of **Cy5-acac**. A mixture of **Cy5-Cl** (1.0 g, 1.6 mmol), 2 mL acetylacetone and 8 mL triethylamine (Et_3N) were added into a round bottom flask with 40 mL DCM. The solution was refluxed for 4 h under N_2. Then the solvent was removed and the solid was dissolved in 30 mL MeOH with 1 mL saturated NH_4PF_6 aqueous solution for 1 h. The solvent was removed by vacuum rotary evaporation. The crude product was purified by silica gel column chromatography using ethyl acetate : acetonitrile (50 : 1 to 10 : 1). The obtained the pure product as green powder (0.8 g, 61.5%). ^{1}H NMR (500 MHz, CD_3CN-d_3) δ 7.55–7.46 (m, 4H), 7.43 (td, J = 7.8, 1.1 Hz, 2H), 7.26 (t, J = 7.5 Hz, 4H), 6.09 (d, J = 14.0 Hz, 2H), 4.12 (q, J = 7.2 Hz, 4H), 3.01 (s, 4H), 1.99 (s, 6H), 1.58 (s, 12H), 1.38 (t, J = 7.2 Hz, 6H). ^{13}C NMR (101 MHz, CD_3CN-d_3) δ 191.55, 170.33, 143.38, 142.22, 141.26, 137.80, 128.65, 124.83, 122.34, 110.67, 104.81, 101.66, 48.97, 39.18, 27.36, 27.16, 22.52, 11.53. HRMS (ESI). Theoretical calc. $C_{38}H_{45}O_2N_2PF_6$ $[M\text{-}PF_6^-]^+$: *m/z* = 561.34756; found: $[M\text{-}PF_6^-]^+$ *m/z* = 561.34491.

Synthesis of Cy5-NO$_2$

To 1.37 g (2 mmol) of **Cy5-acac** and 1.38 g (10 mmol) of *p*-nitroaniline in a 50 mL single-neck flask, 30 mL of toluene was added. The mixture was heated under reflux away from light for 12 hours. After the reaction was completed, a large amount of precipitate was formed. The mixture was filtered to retain the solid, yielding pure blue-violet solid **Cy5-NO$_2$**, 1.15 g, 92%. Blue crystals were obtained by diffusion system of acetonitrile and diethyl ether. ^{1}H NMR (500 MHz, CD_3CN-d_3) δ 8.51–8.47 (m, 2H), 7.88 (s, 1H), 7.79–7.76 (m, 2H), 7.48–7.42 (m, 2H), 7.36 (td, J = 7.8, 1.2 Hz, 1H), 7.14 (td, J = 7.5, 0.8 Hz, 1H), 7.09 (d, J = 7.9 Hz, 1H), 5.70 (d, J = 12.7 Hz, 1H), 3.97 (q, J = 7.2 Hz, 2H), 3.23–3.01 (m, 4H), 2.70 (s, 3H), 2.16 (s, 3H), 1.58 (s, 6H), 1.31 (t, J = 7.1 Hz, 3H). ^{13}C NMR (126 MHz, CD_3CN-d_3) δ 203.89, 167.39, 153.38, 149.00, 146.09, 145.65, 142.68, 141.87, 140.28, 136.65, 128.98, 128.36, 128.32, 125.75, 125.59, 122.92, 122.05, 109.00, 96.49, 47.49, 37.83, 31.50, 28.47, 27.62, 26.11, 17.66, 10.78. HRMS (ESI). Theoretical calc. for $C_{31}H_{32}N_3O_3$ $[M\text{-}I^-]^+$: *m/z* = 494.24382; found: $[M\text{-}I^-]^+$ *m/z* = 494.24402.

Synthesis of Cy5-NH$_2$

To 1.37 g (2 mmol) of **Cy5-acac** and 1.07 g (10 mmol) of *p*-nitroaniline in a 50 mL single-neck flask, 30 mL of toluene was added. The mixture was heated under reflux away from light for 12 hours. After the reaction was completed, a large amount of precipitate was formed. The mixture was filtered to retain the solid. Purification was carried out by silica gel column chromatography using dichloromethane as the eluent, yielding pure reddish-purple solid **Cy5-NH$_2$**, 0.88 g, 75.2%. ^{1}H NMR (500 MHz, CD_3CN-d_3) δ 7.93 (s, 1H), 7.40–7.30 (m, 3H), 7.18–7.12 (m, 2H), 7.09 (td, J = 7.5, 0.7 Hz, 1H), 7.02 (d, J = 7.9 Hz, 1H), 6.90–6.73 (m, 2H), 5.63 (d, J = 12.7 Hz, 1H), 3.92 (q, J = 7.2 Hz, 2H), 3.29–2.98 (m, 4H), 2.68 (s, 3H), 2.19 (s, 3H), 1.57 (s, 6H), 1.27 (t, J = 7.3 Hz, 3H). ^{13}C NMR (126 MHz, CD_3CN-d_3) δ 203.98, 165.89, 152.87, 150.11, 147.27, 142.92, 141.89, 140.02, 138.49, 134.89, 130.57, 129.48, 128.25, 126.77, 126.02, 122.37, 121.98, 114.46, 108.52, 95.56, 46.92, 37.53, 31.41, 28.35, 27.66, 26.19, 17.47, 10.63, 8.18. HRMS (ESI). Theoretical calc. for $C_{31}H_{34}N_3O$ $[M\text{-}I^-]^+$: *m/z* = 464.26964; found: $[M\text{-}I^-]^+$ *m/z* = 464.26965.

X-ray crystallography

Single crystals of **Cy5-NO$_2$** suitable for X-ray diffraction studies were grown by slow vapor diffusion of diethyl ether into acetonitrile solution. Single-crystal X-ray diffraction analysis were performed on a Bruker APEX-II CCD diffractometer with graphite-monochromated Mo K_α radiation (λ = 0.71073 Å) at 293 K, 150 K, and 170 K. All absorption corrections were performed using multiscan. The structure was solved by direct methods and refined by full-matrix least-squares techniques on F^2 with the SHELXL-97 or SHELXL-2014 program package. CCDC 2423384 contains the supplementary crystallographic data of **Cy5-NO$_2$**.

Author contributions

Jiqiang Liu: conceptualization, data curation, investigation, methodology, validation, writing – original draft, writing – review and editing. Abdulkadir Zakari Abdulkadir: data curation, investigation, methodology, and validation. Siye Wu: data curation and investigation. Yonghui Gao: investigation and validation. Baraka Joseph Butuyuyu: investigation and validation. Keith Man-Chung Wong: resources, writing – review and editing. Chi-Sing Lee: resources, writing – review and editing. Lintao Cai: writing – review and editing. Jihong Chen: funding acquisition and resources. Pengfei Zhang: conceptualization, funding acquisition, resources, supervision, writing – review and editing.

Conflicts of interest

There are no conflicts to declare.

Data availability

The data supporting this article have been included as part of the SI.

Supplementary information is available. Details of all NMR spectra, HRMS spectra, XRD information and other spectroscopic results. See DOI: **https://doi.org/10.1039/d5tb00758e**

CCDC 2423384 contains the supplementary crystallographic data for this paper.[42]

Acknowledgements

We are grateful for the financial support from the National Key R&D Programs (China) (2021YFA0910001), Shenzhen Medical Research Fund (D2404002), the National Natural Science Foundation of China (82470719), the Guangdong Provincial Key Area R&D Program (2020B1111540001), the Guangdong Province Basic and Applied Basic Research Fund Enterprise Joint Fund (2023A1515220119), the Shenzhen Science and Technology Program (KQTD20210811090115019), and the Guangdong Basic and Applied Basic Research Fund Project (China) (2019A1515110222 and 2021A1515110699).

References

1 S. Altveş, H. K. Yildiz and H. C. Vural, *Biosci. Microbiota, Food Health*, 2020, **39**, 23.
2 M. Kamel, S. Aleya, M. Alsubih and L. Aleya, *J. Pers. Med.*, 2024, **14**, 217.
3 A. El-Sayed, L. Aleya and M. Kamel, *Environ. Sci. Pollut. Res.*, 2021, **28**, 28926.
4 A. El-Sayed, L. Aleya and M. Kamel, *Environ. Sci. Pollut. Res.*, 2021, **28**, 36967.
5 A.-P. Baciu, C. Baciu, G. Baciu and G. Gurau, *J. Med. Life*, 2024, **17**, 246.
6 F. M. E. Wagenlehner and F. Dittmar, *Eur. Urol.*, 2022, **82**, 658.
7 K. S. Ikuta, L. R. Swetschinski, G. R. Aguilar, F. Sharara, T. Mestrovic and A. P. Gray, *et al.*, *Lancet*, 2022, **400**, 2221.
8 A. Elbehiry, E. Marzouk, A. Abalkhail, M. H. Abdelsalam, M. E. A. Mostafa, M. Alasiri, M. Ibrahem, A. T. Ellethy, A. Almuzaini, S. N. Aljarallah, A. Abu-Okail, N. Marzook, S. Alhadyan and H. M. Edrees, *Front. Microbiol.*, 2025, **16**, 1.
9 E. Sauerborn, N. C. Corredor, T. Reska, A. Perlas, S. Vargas da Fonseca Atum, N. Goldman, N. Wantia, C. Prazeres da Costa, E. Foster-Nyarko and L. Urban, *Nat. Commun.*, 2024, **15**, 1.
10 M. A. Salam, M. Y. Al-Amin, J. S. Pawar, N. Akhter and I. B. Lucy, *Saudi J. Biol. Sci.*, 2023, **30**, 103582.
11 B. Zhang, H. Chen, L. Shi, R. Guo, Y. Wang, Y. Zheng, R. Bai, Y. Gao, B. Liu and X. Zhang, *ACS Sens.*, 2024, **9**, 4560.
12 S. Lepuschitz, T. Weinmaier, K. Mrazek, S. Beisken, J. Weinberger and A. E. Posch, *Front. Microbiol.*, 2020, **11**, 1883.
13 S. Y. Park, S. A. Yoon, Y. Cha and M. H. Lee, *Coord. Chem. Rev.*, 2021, **428**, 213613.
14 M. H. Lee, J. S. Kim and J. L. Sessler, *Chem. Soc. Rev.*, 2015, **44**, 4185.
15 S. A. Yoon, S. Y. Park, Y. Cha, L. Gopala and M. H. Lee, *Front. Chem.*, 2021, **9**, 1.
16 Y. Yao, J. Ma, S. Xing, F. Zeng, L. Wu, Y. Li, J. Du, Q. Yang and Y. Li, *Anal. Chim. Acta*, 2024, **1292**, 342259.
17 N. I. Wickramasinghe, B. Corbin, D. Y. Kanakarathna, Y. Pang, C. S. Abeywickrama and K. J. Wijesinghe, *Biosensors*, 2023, **13**, 799.
18 B. Zhu, X. Xing, J. Kim, H. Rha, C. Liu, Q. Zhang, L. Zeng, M. Lan and J. S. Kim, *Biomaterials*, 2024, **304**, 122419.
19 A. Mukherjee and S. E. Rokita, *J. Am. Chem. Soc.*, 2015, **137**, 15342.
20 M. D. Roldán, E. Pérez-Reinado, F. Castillo and C. Moreno-Vivián, *FEMS Microbiol. Rev.*, 2008, **32**, 474.
21 J. Zhang, M. Zhou, X. Li, Y. Fan, J. Li, K. Lu, H. Wen and J. Ren, *Talanta*, 2023, **254**, 124133.
22 J. Hira, M. J. Uddin, M. M. Haugland and C. S. Lentz, *Molecules*, 2020, **25**, 4949.
23 W. Gao, A. Shi, Y. Hou, P. Zhang, Q. Zhang and C. Ding, *Talanta*, 2025, **290**, 127804.
24 Z. Mi, L. Liu, Y. Zhao and J. Guan, *Int. J. Biol. Macromol.*, 2020, **164**, 932.

25 N. Plumeré, *Anal. Bioanal. Chem.*, 2013, **405**, 3731.
26 D. Yang, H. Y. Tian, T. N. Zang, M. Li, Y. Zhou and J. F. Zhang, *Sci. Rep.*, 2017, **7**, 2.
27 C. Zhang, K. Yan, C. Fu, H. Peng, C. J. Hawker and A. K. Whittaker, *Chem. Rev.*, 2022, **122**, 167.
28 J. J. Morsby, K. M. Atkinson, S. Shradha Reddy Kommidi, T. Freel, H. Janeková, P. Štacko and B. D. Smith, *Eur. J. Org. Chem.*, 2022, e202200270.
29 S. Nisar and B. Sui, *Sens. Diagn.*, 2024, **3**, 1505.
30 A. F. Bedernjak, P. W. Groundwater, M. Gray, A. L. James, S. Orenga, J. D. Perry and R. J. Anderson, *Tetrahedron*, 2013, **69**, 8456.
31 K. A. Bertman, C. S. Abeywickrama and Y. Pang, *ChemBioChem*, 2022, **23**, e202100516.
32 S. Cha, M. G. Choi, H. R. Jeon and S.-K. Chang, *Sens. Actuators, B*, 2011, **157**, 14.
33 K. Jia, Y. Wan, A. Xia, S. Li, F. Gong and G. Yang, *J. Phys. Chem. A*, 2007, **111**, 1593.
34 J. Kabatc and J. Pączkowski, *Dyes Pigm.*, 2004, **61**, 1.
35 F. Bertocchi, A. Delledonne, G. Vargas-Nadal, F. Terenziani, A. Painelli and C. Sissa, *J. Phys. Chem. C*, 2023, **127**, 10185.
36 G. B. Behera, P. K. Behera and B. K. Mishra, *J. Surf. Sci. Technol.*, 2007, **23**, 1.
37 R. R. Nani, J. A. Kelley, J. Ivanic and M. J. Schnermann, *Chem. Sci.*, 2015, **6**, 6556.
38 S. C. Cosgrove, G. J. Miller, A. Bornadel and B. Dominguez, *ACS Sustainable Chem. Eng.*, 2023, **11**, 8556.
39 S. Jiao, S. Yang, X. Meng and C. Wang, *Spectrochim. Acta, Part A*, 2020, **241**, 118637.
40 H. Wang, M. Yang, M. Ji and P. Wang, *J. Photochem. Photobiol., A*, 2022, **427**, 113814.
41 N. A. Turner, B. K. Sharma-Kuinkel, S. A. Maskarinec, E. M. Eichenberger, P. P. Shah, M. Carugati, T. L. Holland and V. G. Fowler, *Nat. Rev. Microbiol.*, 2019, **17**, 203.
42 J. Liu, A. Z. Abdulkadir, S. Wu, Y. Gao, B. J. Butuyuyu, K. M.-C. Wong, C.-S. Lee, L. Cai, J. Chen and P. Zhang, CCDC 2423384: Experimental Crystal Structure Determination, 2025, DOI: **10.5517/ccdc.csd.cc2mbqpd**.